REGULAR PAPER

Effect of Scale and Sequence of Surface Textures on the Anti-adhesive Wear Performance of PVD Coated Tool in Dry Machining SLM-Produced Stainless Steel

Kedong Zhang[1] · Xuhong Guo[1] · Chengdong Wang[1] · Xiangfeng Meng[1] · Lining Sun[1] · Youqiang Xing[2]

Abstract

During the dry post-machining processing of selective laser melting (SLM)-produced stainless steel with TiAlN coated tool, the elements of stainless steel chips can diffuse and adhere into the coated tool surface, causing serious adhesive wear. In this study, to inhibit the adhesion problem at the tool-chip interface, surface textures with different scales (micro-, nano- and micro/nano-textures) are produced on tool rake face by laser processing before and after physical vapor deposition (PVD) TiAlN coatings deposition. To investigate the cutting performance of these developed coated tools, dry machining tests of the SLM-produced stainless steel are carried out. And, the mechanical properties of textured TiAlN coatings such as the hardness, elastic modulus and critical load are also studied to explain the results from the machining tests. It can be found that the anti-adhesive wear performance of TiAlN coated tool is improved by laser surface texturing. The texture dimension significantly affects the mechanical properties and dry cutting performance of the TiAlN coated tool, and the micro/nano-textures are found to be optimum. Meanwhile, the sequence of surface textures also has an effect on the wear performance of the developed TiAlN coated tools. In the experiment, laser surface texturing before coatings is effective in acting as a barrier against flaking of the TiAlN film, providing a higher active surface for the subsequent TiAlN coatings and presenting a higher compressive residual stress. Thus, the developed cutting tool which is textured before TiAlN coatings deposition presents a milder wear compared to the developed one which is textured after TiAlN coatings deposition.

Keywords PVD coatings · Mirco/nano-scale texture · Texture sequence · Selective laser melting

1 Introduction

Selective laser melting (SLM) technique provides an effective and environmental friendly technology for manufacturing complex-shaped parts of stainless steel applied in the bio-medical field. Normally, as a relatively new and continuously evolving technology, the parts produced by SLM technique still suffer from the problems of poor surface finish and low dimensional precision, thus a post-machining process for SLM-produced materials is deemed essential [1]. In the biomedical field, to prevent possible illness or failure of the surgical operation caused by the cutting fluid contaminants, an expensive and time-consuming cleaning steps are usually applied. Dry machining may represent a possible solution to reduce the cleaning steps. However, a harsher friction and wear at the tool-chip interface will be caused by dry machining compared to that caused by wet machining [2], which has provoked the interest in enhancing the machining performance of cutting tool themselves. Due to the characteristics of high hardness and excellent antioxidant properties, PVD TiAlN coatings are currently being deposited on the traditional cemented carbide tool to improve its cutting performance in dry machining of the difficult-to-machine materials. Unfortunately, due to different bond types, thermal expansion coefficient and wettability between the coatings and substrate, PVD TiAlN coated tool still has the problem of insufficient coating adhesion [3, 4].

✉ Xuhong Guo
  xuhongguo@suda.edu.cn

✉ Youqiang Xing
  yqxing@seu.edu.cn

[1] Research Institute of Advanced Manufacturing Technology, School of Mechanical and Electric Engineering, Soochow University, No. 1 Shizi Street, Suzhou 215021, Jiangsu, People's Republic of China

[2] School of Mechanical Engineering, Southeast University, Nanjing 211189, Jiangsu, People's Republic of China

Adhesive wear caused by high contact stress and high friction temperature at the tool-chip interface often causes coatings detachment, resulting in premature tool failure.

To enhance the mechanical properties of PVD coatings and improve the cutting performance of PVD coated tool, various surface technologies have been explored. For example, Pfeiler et al. [5–7] successfully demonstrated that the application of adjusting the coating deposition conditions led to a significant improvement of the properties of TiAlN coatings. The work of Castanho et al. [8] and Kutschej et al. [9], for instance, reported the successful application of optimizing chemical composition and coating architectures to improve the TiAlN coatings' mechanical properties, which was subsequently used as a mould for enhancing the cutting performance of TiAlN coated tool. Based on the above reports, it can be seen that high hardness, excellent abrasion resistance and high corrosion resistance of the TiAlN coatings have been obtained by adjusting the coating preparation process, which indicates that the preparation technology of PVD coatings has been relatively perfect. Although the mechanical properties have been improved, TiAlN coatings still suffer from the problems of high internal stress and poor adhesive strength. Thus, the effect of adjusting the coating preparation process on further improving the mechanical properties of the TiAlN coatings is limited, especially for enhancing the coating adhesion.

As the coating adhesion is important for all PVD coatings, the study on improving the adhesive strength between the coatings and substrate has received significant attention over the years. Kromer et al. [10] proved that increasing the substrate roughness can effectively enhance the adhesion of PVD coatings due to the improved mechanical interlocking at the coatings-substrate interface. However, the conventional method of substrate roughening, i.e. grit blasting, has the disadvantages of environmental and operator health risks. Besides substrate roughening, applying a thin adhesive interlayer between the coatings and substrate is also used. For example, Li et al. [11] applied a Ti interlayer in PVD WS$_2$/TiSiN soft-hard composite coatings to form the metallurgical bond between the carbide substrate and TiSiN hard-coatings, which could thereby improve the coating adhesion. Nevertheless, in spite of its widespread use and efficiency, applying the adhesive interlayer is a complex control process and has high requirements for equipment conditions. Buchwalder et al. [12] stated that the chemical bonding properties at the coatings-substrate interface, specific surface area and surface energy of the substrate are the important factors influencing the adhesive strength between the coatings and substrate. Meanwhile, Tillmann et al. [13] found that a high specific surface area and surface free energy can be obtained through optimizing the morphology and parameters of the micro/nano-structure patterns fabricated on the substrate surfaces,

which was benefit for the coatings deposition. Recently, in the field of PVD tool coatings, there have been increasing researches to improve the coating adhesion by laser texturing [14–16]. As a method to produce multimodal roughness and high curvature of texture elements, laser surface texturing (LST) can modify the morphology and physicochemical properties of both the substrate and coatings surface and include various sequential processing steps. Yuan et al. [17] produced micro-scale dimple textures with different densities on the zirconium coatings surface and studied the tribological performance of these textured samples. Results showed the tribological behavior of the textured samples was significantly improved compared with the untextured one. Neves et al. [18] fabricated micro-textures on the substrate surface of TiAlN coatings using a Nd:YAG laser under different processing parameters and found that the coatings with a textured substrate surface exhibited a higher coating adhesion. Thus, the improved machining performance of the PVD coated tool was obtained by the laser textured substrate in the turning experiments. Similarly, to alter the tool-chip interaction during cutting processing, Viana et al. [19] used a nanosecond laser to texture the cemented carbide substrate of PVD coatings and found that the cutting performance of coated tools was obviously improved by the textured substrate. To inhibit the adhesion problem at the tool-chip interface under the condition of dry cutting, nano-scale textures were produced on the rake face of DLC coated tool using a femtosecond laser and the influence of different texture direction were also studied [20, 21].

So far, most of the researches about the textured cutting tools aimed at altering the tool-chip interaction during cutting processing, and the advantages of these surface textures in anti-adhesion and friction-reduction are mainly attributed to several physical mechanisms such as the effects of retaining cutting fluids, trapping wear debris, reducing the contact area, and stabilizing an adhesion layer at the tool-chip interface. However, to fully take advantage of PVD coatings, the sufficient adhesive strength between coatings and substrate is crucial. To the best knowledge of the authors, the study about the effect of laser surface texturing on the PVD coating adhesion is limited, and the influence of dimension and sequence of surface textures on the coating adhesion and cutting performance of the coated tools has not been investigated. In addition, few studies aim at improving anti-adhesive wear properties of coated tools during dry cutting of SLM-produced stainless steel. In this study, the PVD TiAlN coated tools with different scale textures on the substrate or coatings surface are prepared. The dependence of anti-adhesive wear performance on texture dimension and sequence is studied through dry cutting tests of SLM-produced stainless steel with these developed coated tools. To verify the adhesive strength of the coatings and explain the

results from the machining tests, the mechanical properties of the coated samples are characterized by nanoindentation, XRD and scratch tests.

2 Experimental

2.1 Preparation of Samples

2.1.1 Fabrication of SLM-Produced Parts

To produce the stainless steel by SLM technique, commercially gas-atomised AISI 316L (UNS S31603) spherical powder with size fraction of 20–73 μm is used, the SEM picture of which is presented in Fig. 1a. The corresponding chemical composition of this powder is presented in Table 1. The manufacturing of stainless steel workpieces is performed on a SLM Realizer II 250 machine (MPC-HEK) equipped with a continuous wavelength Ytterbium fiber laser (spot size 200 μm, maximum power 400 W), the details of which are described in Ref. [22]. Figure 1b illustrates the schematic drawing of experimental set-up for SLM processing and the surface topography of SLM-produced stainless steel is observed by a scanning electron microscope (SEM). The SEM image in Fig. 1c reveals the typical shortcomings of SLM-produced samples like high surface roughness, low dimensional accuracy and surface quality, which is due to the melting channel overlapping,

Fig. 1 Principle of SLM processes: **a** the AISI 316L stainless steel powders, **b** a sketch for the SLM, and **c** micrographs of the SLM-produced stainless steels [22]
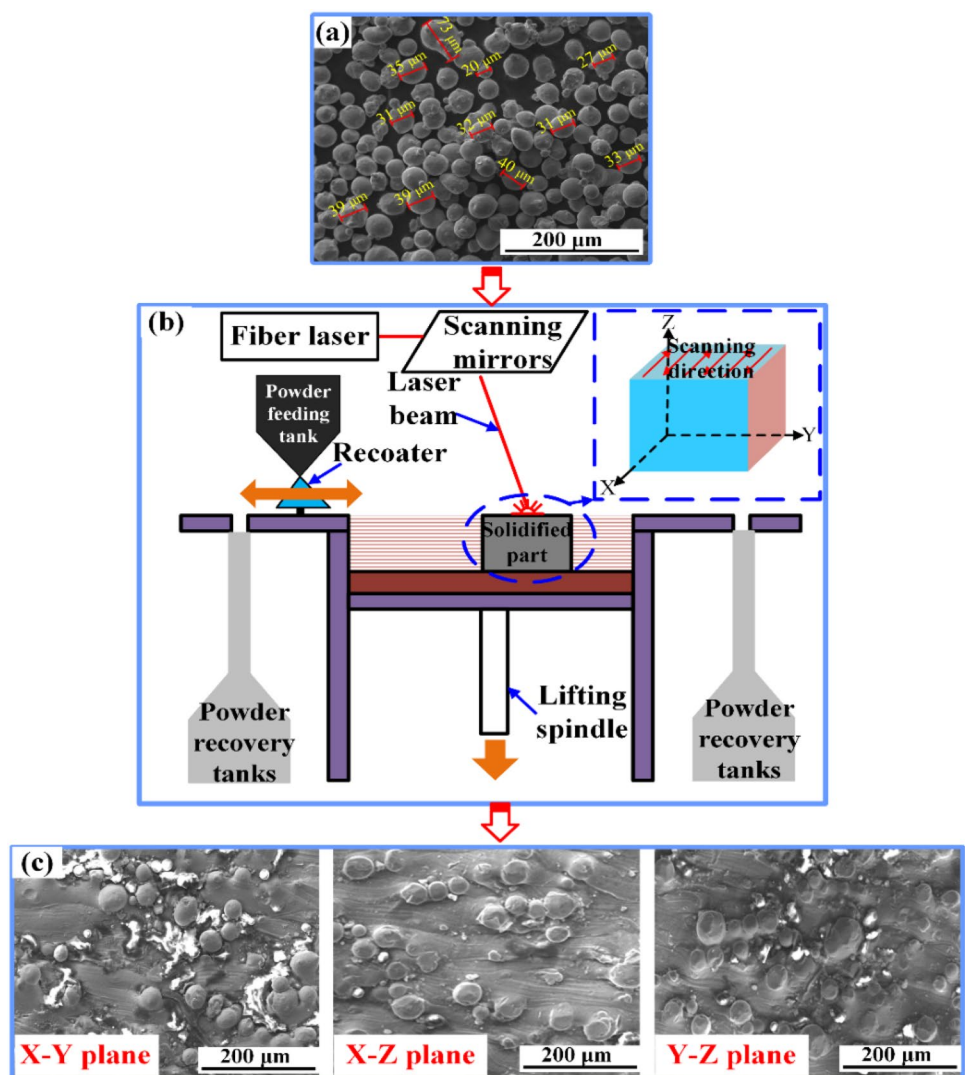
Table 1 Chemical composition of the as-received 316L powder

Element	Fe	Cr	Ni	Mo	Mn	Si	N	C	P	S
wt.%	Balance	16.69	10.16	3.02	1.71	0.54	0.07	0.02	0.013	0.01

unmelted powders adhesion and interlayer bonding during the SLM processing.

Figure 2 shows the X-ray diffraction patterns of the precursor powders and typical SLM-produced samples. All the diffraction peaks can be indicated as austenitic stainless steel. Although the SLM processing can cause rapid solidification of AISI 316L powder, both precursor powders and SLM-produced materials are composed by the γ (fcc) austenite phase with a small part of δ (bcc) ferrite. The SLM process can induce the residual stresses and lattice distortion on the produced materials, thus the diffraction peak of SLM-produced samples broadens, which agrees with that reported by Zhong et al. [23].

2.1.2 Fabrication of Different Scale Textures and TiAlN Coatings

Prior to the deposition of TiAlN coatings, WC–Co (6 wt% Co) cemented carbide, which is usually as tool material, is
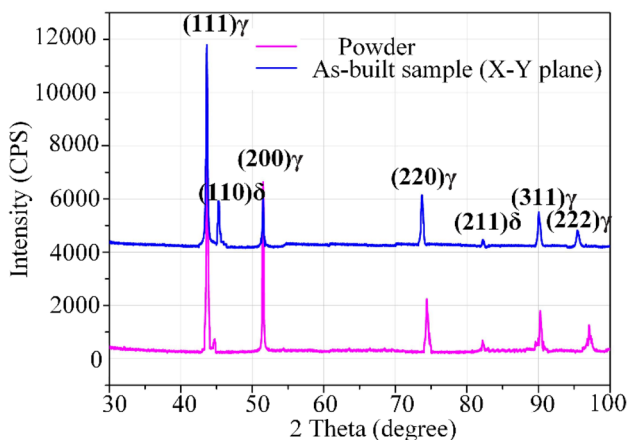

Fig. 2 XRD spectra of the precursor powders and typical SLM-produced samples

selected as the substrate in this study. Detail about the polishing treatment for obtaining a super smooth surface has been described in Ref. [22]. To induce the micro-textures on the WC/Co substrate and TiAlN coatings surface, a nanosecond pulsed laser (Nd:YAG, pulse duration 10 ns, wavelength 1064 nm, repetition frequency 20 kHz) is utilized to fabricate linear grooves on the tool rake face (depth of ~ 10 μm, width of ~ 20 μm and period of ~ 200 μm). And, a femtosecond laser (Ti:sapphire regenerative amplified laser system, pulse width 120 fs, wavelength 800 nm, repetition rate 1 kHz) is utilized to produce the nano-textures on the tool surface (depth of ~ 150 nm and period of ~ 550 nm). The processing parameters of nanosecond and femtosecond laser are shown in Table 2, and the distance between the textured area and main cutting edge is ~ 150 μm.

Cathode arc-evaporation technique is used to deposit TiAlN films on the substrate surface without employing any interlayer, the schematic diagram of which is presented in Fig. 3. The details of the coating setup are presented in Ref. [24]. Before coatings deposition, the base pressure of chamber is controlled below 7.0×10^{-3} Pa, then N_2 gas is introduced into the chamber. TiAlN coatings are deposited for 100 min using two Ti and two TiAl composite targets, and the average coating thickness of ~ 3.0 μm is obtained.

In order to evaluate the effect of dimension and sequence of surface textures, six different types of textured samples are prepared, and the schematic illustrations of these textured TiAlN coated tools are presented in Fig. 4. For simplifying the nomenclature, the developed cutting tools, which are textured before TiAlN coatings deposition, are named TC. And the developed cutting tools, which are textured after TiAlN coatings deposition, are named CT. The TC and CT tools with micro-textures are named TC-M and CT-M, respectively. Similarly, the TC and CT tools with nano-textures are named TC-N and CT-N, respectively. And, the TC and CT tools with micro/nano-textures are named TC-MN

Table 2 Processing parameters of the nanosecond and femtosecond laser on different surface

Scale of textures	Nanosecond laser				Femtosecond laser			
	Current (V)	Speed (mm/s)	Frequency (kHz)	Times	Pulse energy (μJ)	Speed (μm/s)	Scanning space (μm)	Times
Micro-texture on substrate	5	15	7	2	–	–	–	–
Nano-texture on substrate	–	–	–	–	2.5	500	5	1
Micro/nano-texture on substrate[a]	5	15	7	2	2.5	500	5	1
Micro-texture on coating	7	10	7	2	–	–	–	–
Nano-texture on coating	–	–	–	–	3	400	5	1
Micro/nano-texture on coating[a]	7	10	7	2	3	400	5	1

[a]To fabricate the micro/nano-textures, nanosecond laser is firstly used to form the micro-grooves, then nano-textures are induced on the micro-textured surface using the femtosecond laser

Fig. 3 The schematic diagram of cathode arc-evaporation technique
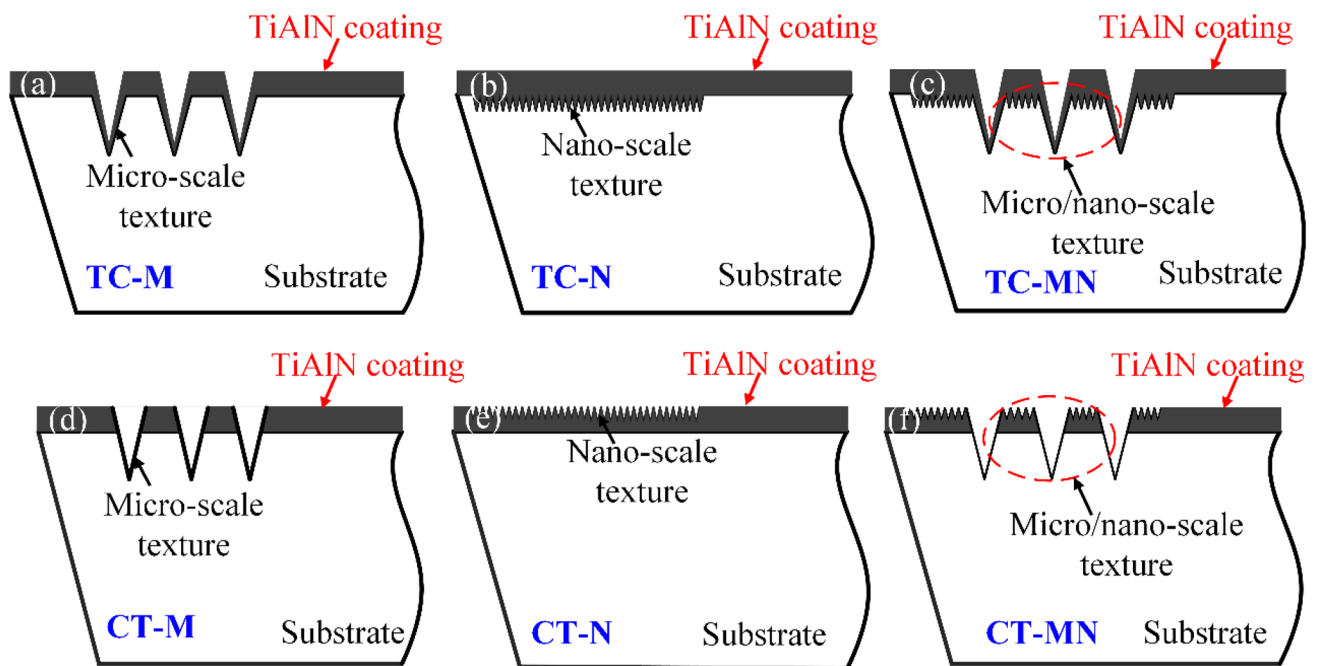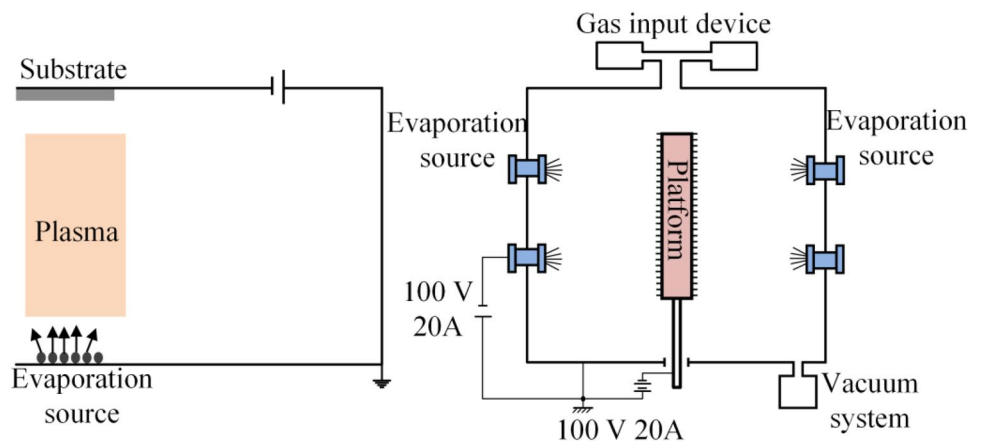

Fig. 4 Schematic representation of the different textured TiAlN coated tools

and CT-MN, respectively. The TiAlN coated tool without laser textures (named CC) is also prepared for comparison.

2.2 Testing and Characterization

The surface morphology and corresponding elements compositions and distributions on the different TiAlN coated specimens are observed by a scanning electron microscope (SEM, QUANTA FEG 250) equipped with energy dispersive X-ray spectroscopy (EDS). EDS mapping, which shows the elements and their locations as bright colors in mapping images, is used to get a better view of the distribution of elements on wear tracks. High concentration of a certain element can be seen as a high contrast in the mapping image. Atomic force micro-scope

(AFM) is performed to measure the depth and period of the uniform nano-textures. For examining the crystallization and residual stress of the samples, a two-dimensional X-ray diffraction (XRD) system using a Bruker D8 Discover instrument with cobalt radiation is utilized. Meanwhile, a LEPTOS software is used to calculate the residual stress on (220) crystallographic plane. A Micro Materials NanoTest System is also used to estimate the mechanical properties of the coatings. And, during the nanoindentation test, the maximum load is controlled below 5000 mN, which could achieve the indentation depths less than 10% of the total thickness. The hardness and elastic modulus of each sample are measured ten times by an indenter with Φ10 μm spherical shape to get an average value. During the processes of nanoindentation test, the

Table 3 Cutting conditions

Workpiece	AISI 316L stainless steel produced by SLM technology
Cutting tool	PVD TiAlN coated tool
Tool geometry	Rake angle $-5°$; clearance angle $5°$; inclination angle $0°$; side cutting edge angle $45°$
Cutting speed	50–200 m/min
Cutting depth	0.5 mm
Feed rate	0.2 mm/rev
Cutting fluid	Dry cutting

Table 4 Mechanical properties of the SLM-produced 316L stainless steel (X–Y plane)

316L stainless steel	Young's Modulus (GPa)	Ultimate tensile strength (MPa)	Yield strength (MPa)	Elongation (%)
SLM	195 ± 60	692 ± 40	457 ± 54	28 ± 6

load–displacement indentation curves are recorded to evaluate the hardness and elastic modulus of the coated samples based on the Oliver–Pharr method.

To evaluate the bond strength of PVD TiAlN coatings to the substrate, the scratch tests are performed by an MFT-3000 device, and a 200 μm radius diamond Rockwell 'C' stylus is used in the scratch test. A normal load range of 0–120 N, a scratch travel of 4 mm and a load increase rate of 150 N/min are selected in this experiment. To determine the coating adhesion, the friction coefficient and acoustical signal are recorded continuously during the processes of scratch tests. After the scratch tests, the wear tracks formed by the penetrator are observed by a white light interferometer.

To evaluate the anti-adhesive wear properties of the developed coated tools in dry cutting of SLM materials, cutting tests are performed on a lathe (CA6140, China). The cutting conditions are presented in Table 3. As the workpiece materials, a round bar of AISI 316L stainless steel with external diameter 60 mm is produced by SLM technique under the operational parameters of Sect. 2.1.1, the main mechanical properties of which are listed in Table 4. All turning tests are repeated five times to guarantee the results' accuracy. After the machining test, the morphologies and chemical composition of wear track on the coated tool surface are observed by SEM/EDS to analyze the wear behaviors of various textured tools.

3 Results and Discussion

3.1 Characteristics of the TiAlN Hard-Coatings and Laser Textures

Figure 5 shows the SEM images of the different textured tools. For the micro-textured coated tool (TC-M), a micro-groove structure with depth ~ 10 μm, width ~ 20 μm and period ~ 200 μm is observed, which inherits the geometry of micro-grooves fabricated on WC/Co substrate surface. Around the groove boundaries, no discontinuities and cracks of the TiAlN coatings are observed. Moreover, the TiAlN coatings on the micro-textured sample are continuous and integrated, exemplified by the cross section of the groove in Fig. 5a that the TiAlN coatings have been successfully deposited onto the bottom and sidewall of micro-scale groove. Well known, during laser irradiation the Co binder phase of substrate surface can be rapidly melted and evaporated, which results in the thermal stresses; thus, microcracks are formed and observed in the resolidified WC, as shown in the cross section of the groove in Fig. 5a. In the nano-textured TiAlN coatings of Fig. 5b (TC-N), from the top view the periodic nano-ripple structures induced by the femtosecond laser on the substrate are fully covered by the coatings. Additionally, the micro- and nano-textures can act as a barrier against slipping of the TiAlN film, which is well demonstrated by that the TiAlN coatings material has penetrated into the grooves, as shown in the cross-sectional image. It is worth mentioning that the fracture surfaces morphology of PVD TiAlN coatings is changed from a clear columnar structure to a predominantly glass-like structure due to the laser substrate pretreatment (the insets of Fig. 5a, b). As reported by Rossnagel et al. [25], the atomic migration and nucleation rate of the coatings can be promoted by an increased surface activity of the laser textured substrate. Thus, the growth of columnar structure is inhibited during the deposition processing of TiAlN films, which can lead to the dense coatings. In addition, the laser textured substrate surface with more concave and convex micro- or nano-structures is more suitable for cathode arc-evaporation and the deposition rate is faster on the textured area. Thus, the microstructure of the PVD TiAlN coatings is influenced by the laser surface textures. The combined effects caused by the nanosecond and femtosecond laser surface texturing, such as low amount of Co phase, even and rough substrate surface and densification of the PVD coatings, are all presented on the TC-MN tool, as shown in Fig. 5c.

Figure 5d–f show the two-dimensional SEM images of the three different coated tools (CT-M, CT-N and CT-MN), which are textured after TiAlN coatings deposition. As
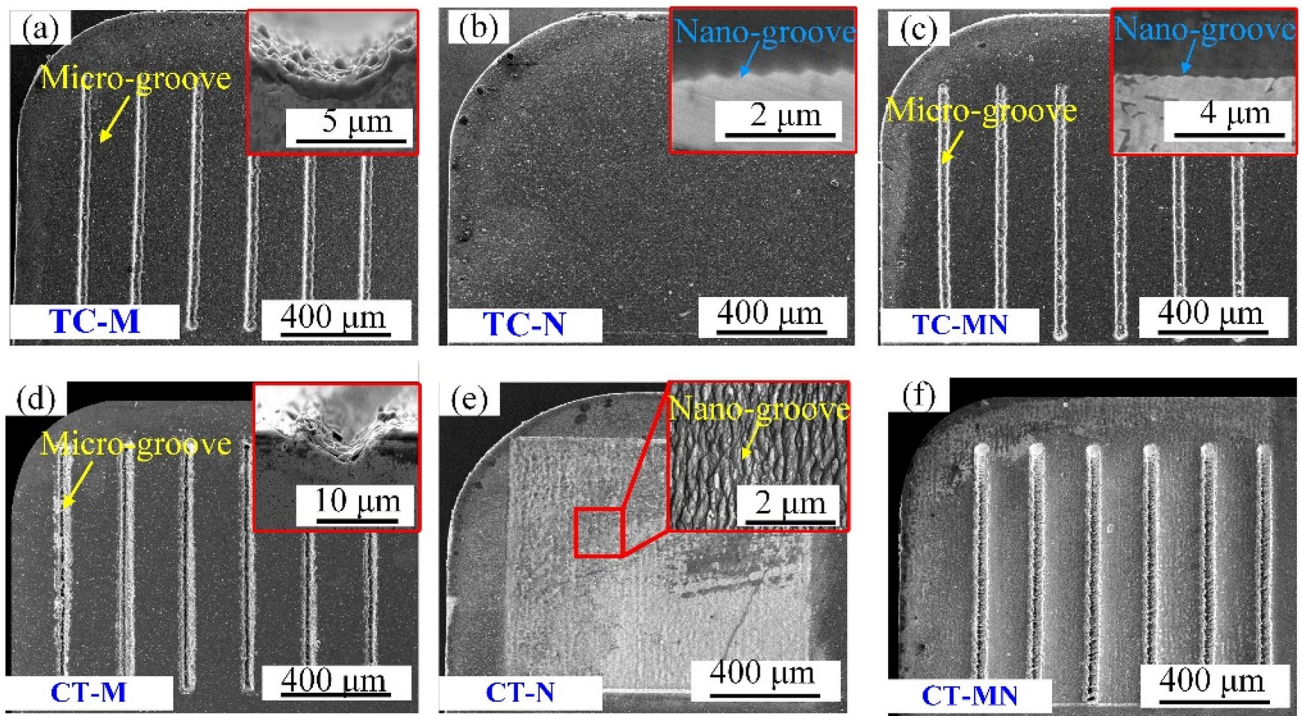
Fig. 5 SEM images of the different rake-face textured TiAlN coated tools

shown in Fig. 5d, the micro-grooves sizes formed on TiAlN coatings surface are basically consistent with that on the WC/Co substrate. However, due to melting and ablation of the coating materials caused by nanosecond laser processing, the TiAlN coatings of CT-M tool on the textured area are cracked and partiality delaminated, exposing the WC/Co substrate. The structure profile of micro-textures is rough, confirming the existing of accumulated materials. The SEM analysis of CT-N tool reveals that periodic slender granular ripples structures with depth of ~ 150 nm and period of ~ 550 nm are successfully fabricated on the TiAlN coatings surface, the formation of which is due to the exciting of surface plasmon polaritons caused by the femtosecond laser irradiation [26]. To note, because of the ultra-short laser pulse and ultra-high peak laser intensity, the femtosecond laser texturing on the TiAlN coatings induces less pronounced thermal effects and the coatings surface is well preserved without collateral damage.

3.2 Characterization of Coating Mechanical Properties

To investigate the cutting performance of the developed coated tools and explain the results from the machining tests, it is necessary to basically explore and understand their mechanical properties. The mechanical properties of TiAlN

coted samples are characterized by nanoindentation, XRD and scratch test. Figure 6a–d present the hardness and elastic modulus of CC, TC and CT sample measured by nanoindentation. It reveals that the laser surface texturing before and after coatings has both a minor effect on hardness and elastic modulus values of TiAlN coatings. To note, the textured TiAlN coatings exhibit a little higher hardness and lower elastic modulus in comparison with the conventional one, which is in agreement with Zhang et al. [27]. Grain growth corresponding to a predominantly glass-like structure could contribute to this increase of the hardness.

To study the adhesive behavior of TiAlN coatings, the critical load is measured during the scratch test at which the coatings peel off and WC/Co substrate is exposed. As seen in Fig. 6e, f, the laser surface texturing after coatings has a minor effect on the coating adhesion, while the laser surface texturing before coatings significantly enhances the adhesive strength between the coatings and substrate. To further confirm the difference between the adhesive behavior of CC, TC and CT samples, the 3D profiles and SEM images of the wear tracks formed on the different coated samples after the scratch tests are presented in Fig. 7. The 3D profile of CC samples in Fig. 7a shows that at the beginning of the wear/scratch track there are discontinuous points of the coatings detachment. As the rubbing continues, the TiAlN layer is scraped off and WC/Co substrate is exposed leading to the stylus-on-carbide contact, as shown in the
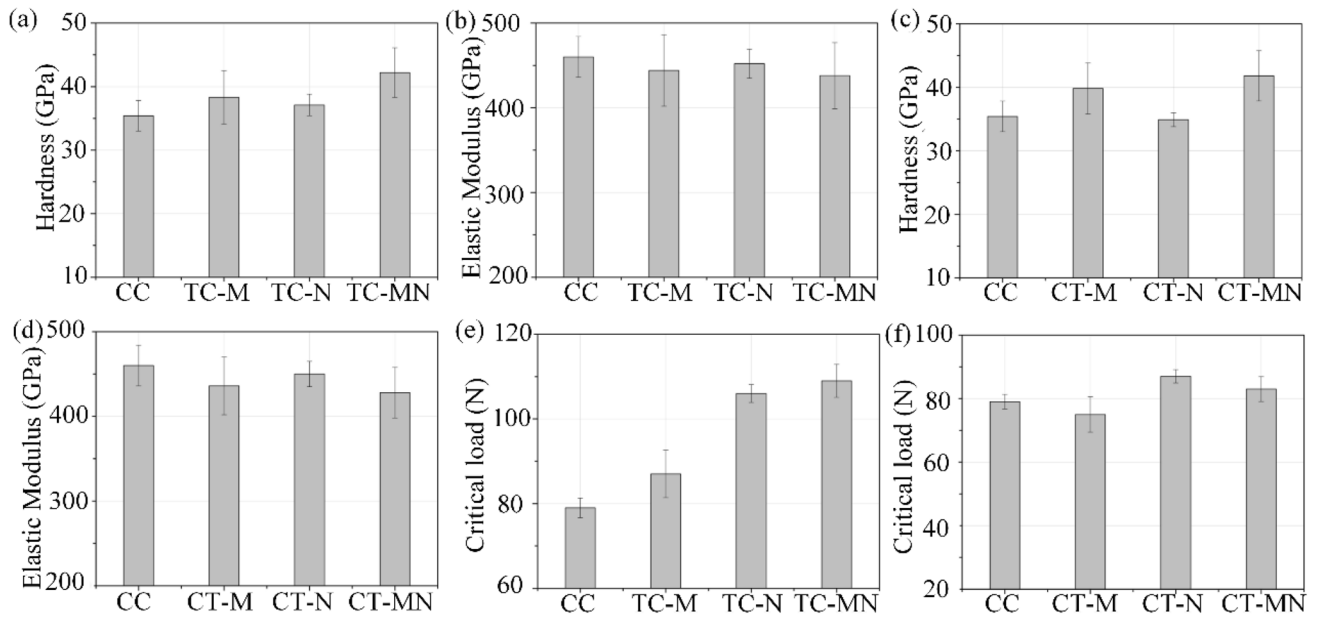
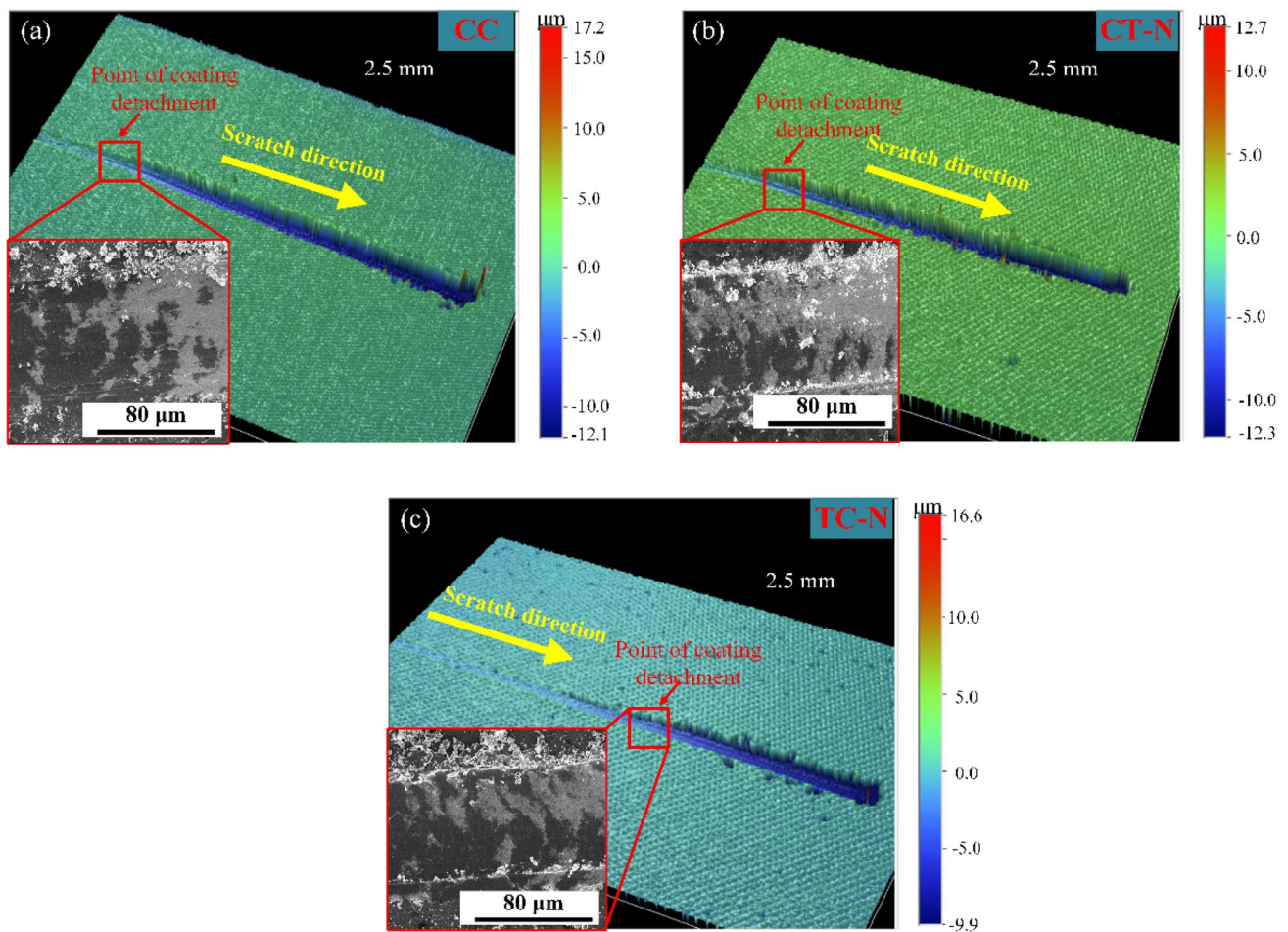**Fig. 6** Hardness, elastic modulus and coating adhesion of the different textured TiAlN coated tools

Fig. 7 The 3D profiles and SEM images of the wear tracks formed on **a** CC, **b** CT-N and **c** TC-N samples after the scratch tests

SEM image of Fig. 7a. The coating's "practical adhesion" is determined by the normal load i.e. the critical normal load before the occurrence of continuous coatings detachment, which corresponds to the beginning of diamond stylus-on-carbide contact, as reported by Viana et al. [19]. The 3D profile and SEM image of CT-N sample in Fig. 7b shows the coatings delamination, with exposure of the cemented carbide substrate, which indicates a similar wear track compared with the CC sample. However, for the TC-N sample, the failure mode spreads further away from the scratch track until total coatings delamination, under the same experimental conditions. Thus, the wear track of TC-N sample in Fig. 7c indicates a better coating adhesion compared to that of CC and CT-N samples, which is in agreement with the result about the coating adhesion in Fig. 6e, f. The other researchers [28, 29], who studied the adhesive strength of the coatings with laser textured substrate, found that a clean, degassed and activated substrate surface can be obtained by the bombardment of laser beam, which led to relatively low crystallographic mismatches between the deposited metal nitride coatings and textured substrate. It is also worth mentioning that, due to the combined beneficial effects caused by the micro- and nano-textures, the TC-MN sample shows the best coating adhesion compared to the TC-N and TC-M samples.

In addition, the coating adhesion is also believed to be related with residual stresses of the substrate surface. Thus, to study the possible mechanisms for the effects of laser surface texturing, the residual stresses of the different textured substrates are measured by XRD and the results are shown in Fig. 8. It can be seen that all the laser textured substrates are in a compressive residual stress state and under higher residual stress compared to the conventional one, which is expected from the nature of the laser processing. To note,
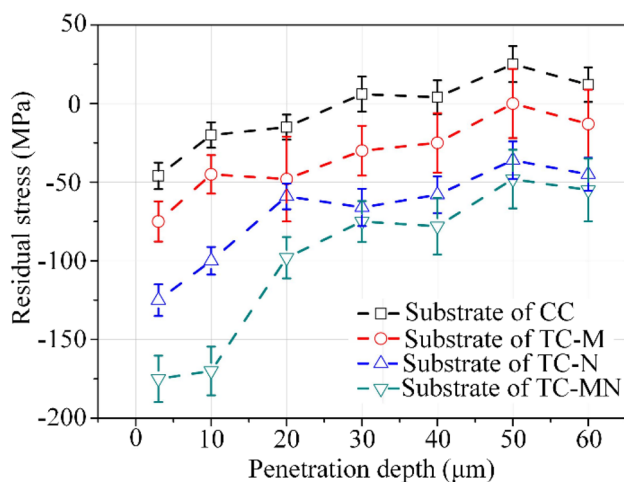
the compressive residual stress in near to the micro-/nano-textured substrate surface is higher than that in the only nano- or micro-scale textured one, indicating that the laser processing significantly influences the stress state of the substrate. As the penetration depth increases to 60 µm, different residual stress state is also detected on the various substrates, which is due to the different penetration depth of laser pulse and different temperature of WC/Co substrate during various laser processing modes.

3.3 Effect of Texture Dimension and Sequence on Wear Behavior

3.3.1 Wear Track of TiAlN Coated Tool Without Textures

Figures 9 and 10 show the typical SEM images of wear track on the rake and flank faces of CC tool after cutting for 1, 3, 4, 5 min. And, the corresponding EDS analyses are presented in Fig. 11. As shown in these figures, adhesive wear is observed and gets worse with the increasing cutting time. The conventional TiAlN coated tool presents significant wear even after 1 min, and from a closer look the WC/Co substrate exposes on the wear track. As cutting time goes on, an adhesion layer is found on the worn rake face after 3 min, indicating the adhesion of stainless steel to the tool rake face. Moreover, when the cutting time reaches 4 min, chipping of the cutting edge occurs along with adhesion layer flaking (Fig. 9). In addition, the workpiece material severely adheres to the exposed area again after 5 min cutting, as shown in Fig. 10, indicating the repeated recycling process about flaking and reformation of the adhesion layer on the tool surface. If the workpiece adhesiveness to the tool surface is higher than the adhesive strength between the coatings and substrate, the spalling of coatings will occur.

To better understand the formation of adhesive wear, EDS mapping analysis on the tool worn area is carried out at different cutting times. The EDS mapping in Fig. 11 shows the element distributions (Ti, W and Fe) of the worn area of the tool rake face at different cutting times. After 1 min cutting, the W element is presented on the too-chip contact area, which indicates the WC/Co substrate exposes on the wear track. When the cutting time reaches 3 min, EDS mapping shows high amounts of Fe element and decreased cemented carbide levels on the too-chip contact area, which indicates the adhesion of stainless steel to the tool rake face. As cutting time goes on, EDS shows the detachment of TiAlN coatings occurs along with the flaking of the adhesion layer. Thus, the EDS mapping in Fig. 11 further confirms that the TiAlN coatings on the rake face retreat significantly by the above-mentioned cycles.

Moreover, the progression of flank wear with the increasing cutting time is also presented in Fig. 9. The abrasive wear is observed on the tool flank face and exacerbated as
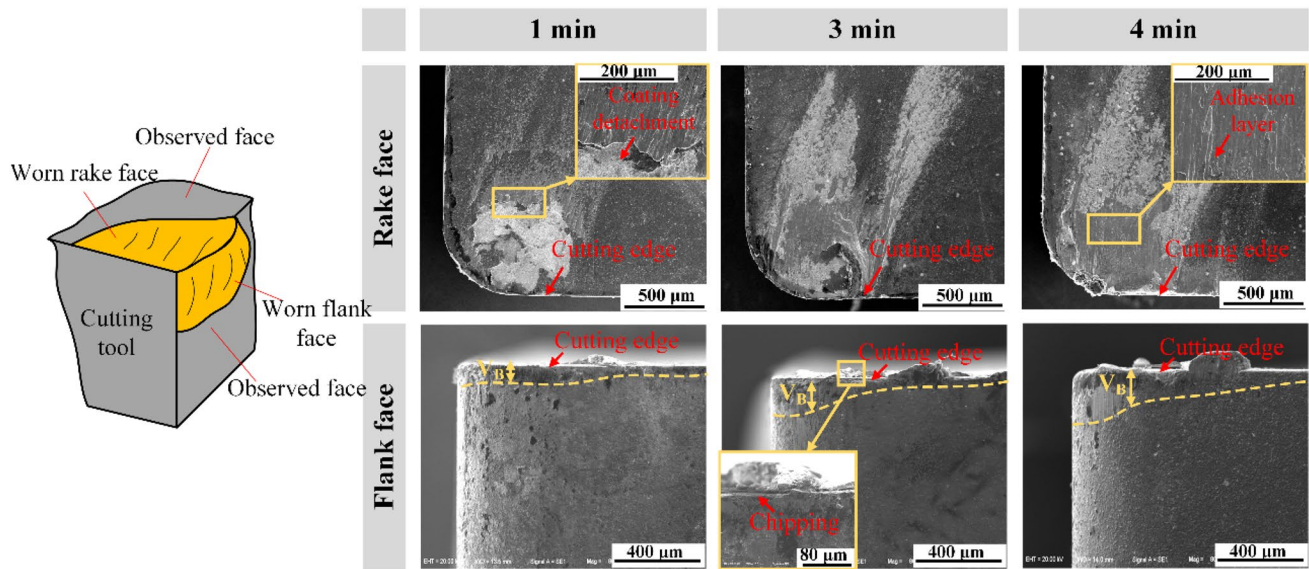
Fig. 8 Residual stress profile on the substrate surfaces after various laser pretreatments

Fig. 9 SEM micrographs analyses of the rake face and flank face of CC tool after 1, 3 and 4 min cutting at speed of 200 m/min

the increasing of cutting time. Subsequently, the built-up edge (BUE) is formed at the tool cutting edge, which brings about the fatal damage of the TiAlN coatings and great tool wear.

3.3.2 Wear Behavior of the Developed TiAlN Coated Tools

The typical SEM images of wear track on the rake faces of TC-M, TC-N and TC-MN tools after cutting for 3 and 5 min are presented in Fig. 12, which indicates a milder chip adhesion on the rake face of the TC tools compared to that of CC tool. The significant difference between the textured and untextured TiAlN coated tools lies in the area of coatings detachment, which is less extensive in the case of TC

Fig. 10 SEM micrographs analyses of the rake face of CC tool after 5 min cutting at speed of 200 m/min

tools compared to the CC tool. According to the SEM image of TC-M tool, coatings detachment is also observed around the micro-scale grooves after 3 min cutting. Since the direction of friction force at the tool-chip interface is orthogonal with the groove direction, the micro-grooves may be a starting point for crack formation, arousing and accelerating detachment of TiAlN coatings around the grooves. This is the negative effect caused by the micro-textures on the substrate surface. However, the micro-grooves can also hook the workpiece material and create stable protective adhesion layer on the tool rake face, as shown in the SEM image of TC-M tool after 5 min cutting, which is the advantages of the micro-textures. In this case, the overall benefit effect due to the textures is obtained, because under the same cutting condition the coatings detachment of TC-M tool is smaller than that of CCT tool, as shown in Figs. 10 and 12. Thus, the positive effect of the micro-texture exceeds its disadvantages of promoting crack initiation. For the TC-N tool, a lesser degree of adhesive wear occurs as evidence from the much smaller exposed substrate areas, compared to the conventional TiAlN coated tool. The surface morphology of adhesive wear on tool rake face is an excellent indicator of the coating adhesion. A lesser coatings detachment probability can be correlated to a higher coating adhesion.

Figure 13 shows similar SEM images for CT-M, CT-N and CT-MN tools. For CT-M tool, the severer coatings detachment is taking place compared to CC tool after 3 min cutting, which is an indication of lower coating adhesion. As the cutting time increases, the wear debris are collected by the micro-grooves and a stable adhered layer of workpiece materials is formed on the rake face of CT-M tool, which can act as a lubricant and protect the tool from wear. In the
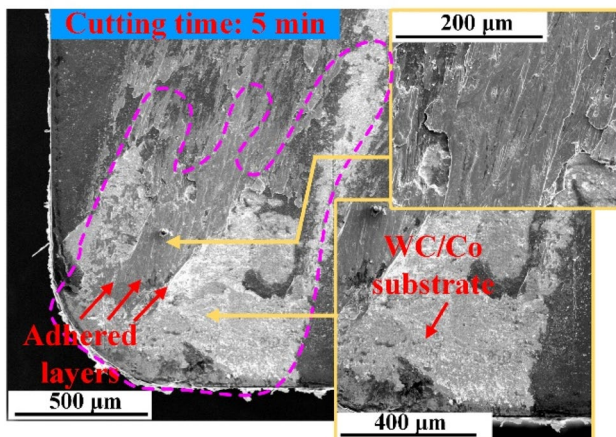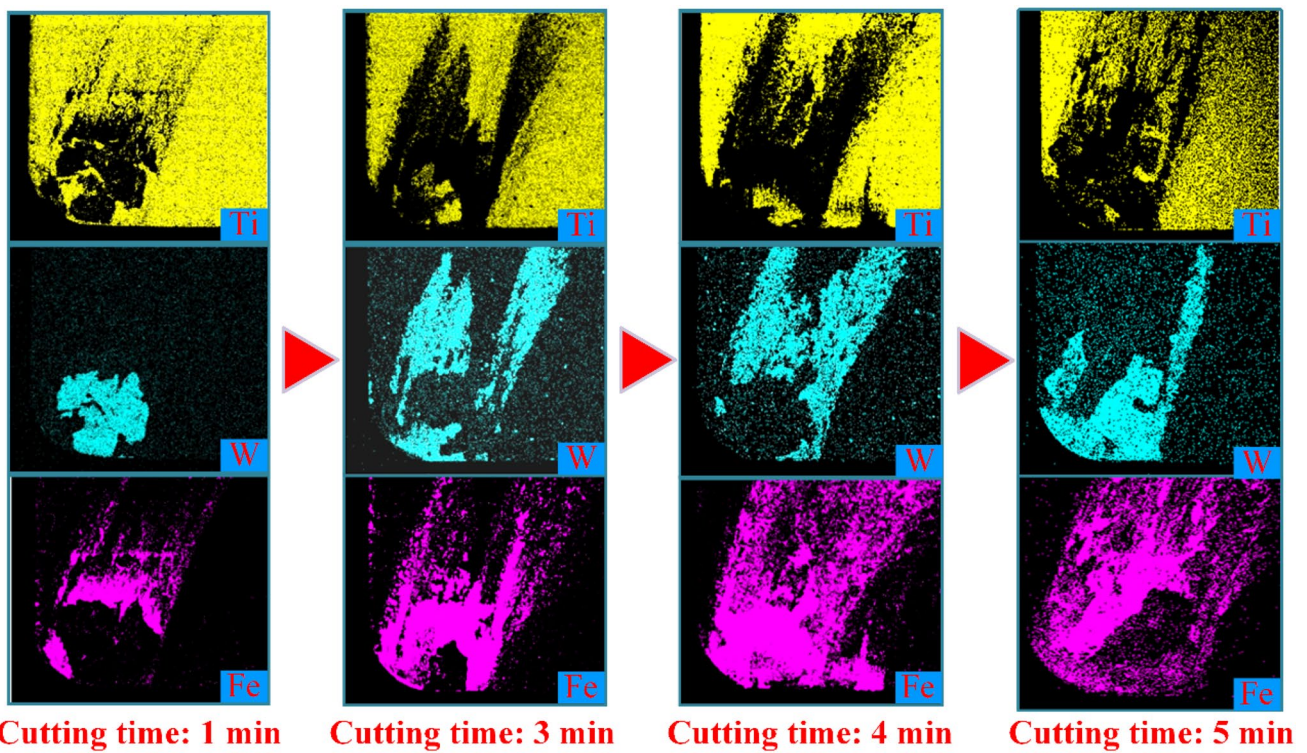
Fig. 11 EDS analyses of the rake face of CC tool after 1, 3, 4 and 5 min cutting at speed of 200 m/min
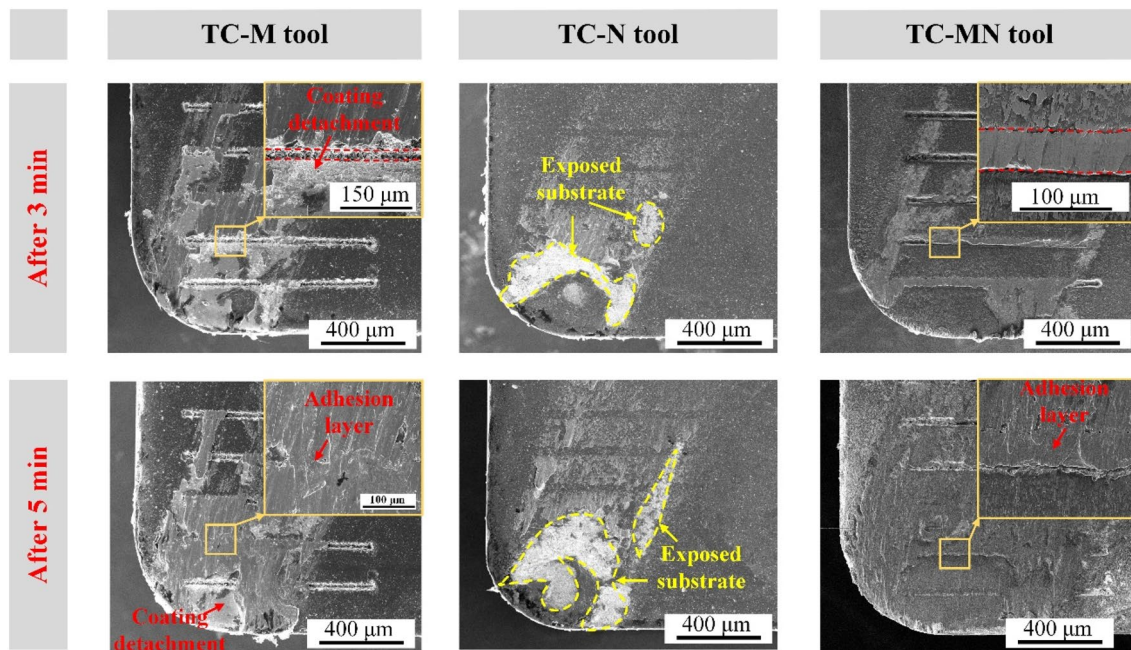

Fig. 12 SEM micrographs analyses of the rake face of TC tool after 3 and 5 min cutting at speed of 200 m/min

case of CT-N tool, the rake face presents a milder wear in comparison with CC tool. After 3 min cutting, the enlarged micrograph of wear area shows that there also exists some workpiece adhesion, most of which is distributed on the nano-textured region. Part of nano-ripple structures induced by the femtosecond laser is still visible after 5 min dry
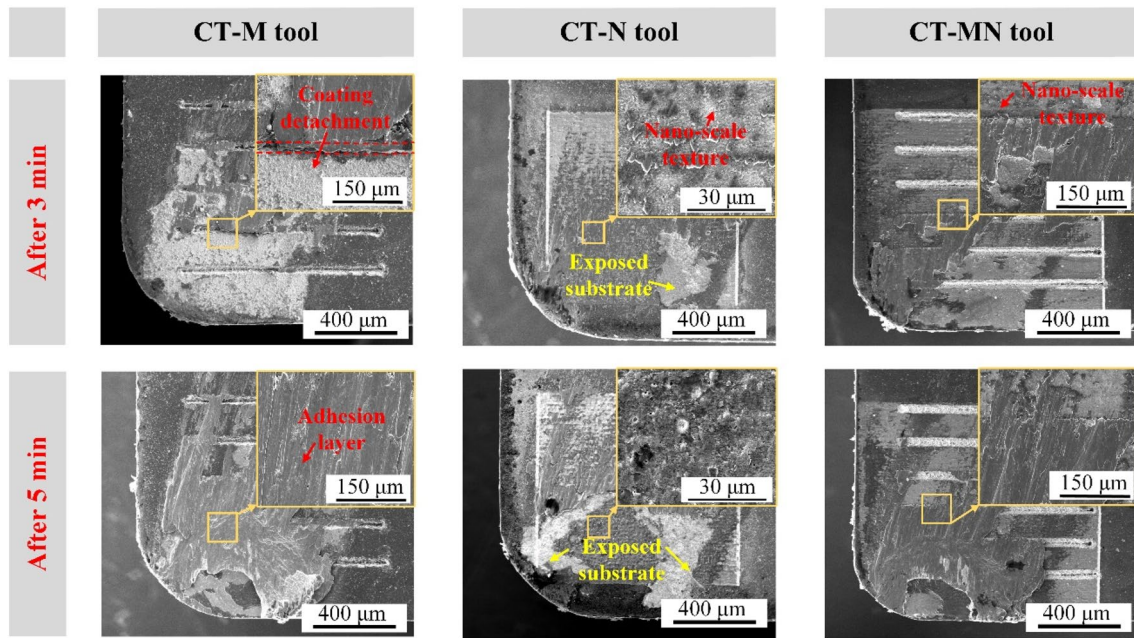
Fig. 13 SEM micrographs analyses of the rake face of CT tool after 3 and 5 min cutting at speed of 200 m/min

cutting. However, the coatings around the cutting edge seem to have been fragmented and plucked off, indicating that the nano-textures fabricated on the coatings surface cannot effectively improve the coating adhesion. The steel adhesion phenomenon on CT-MN tool is similar with TC-MN tool. However, there is a difference about coatings detachment between the CT-MN and TC-MN tools. CT-MN tool possesses larger area of coatings detachment than TC-MN tool, clearly indicating the influence of texture sequence on the anti-adhesive wear properties.

To visually investigate the machining performance of the different cutting tools, the flank wear land width VB_{max} of various TiAlN coated tools as a function of cutting distance are analyzed. Clearly, a lower VB_{max} occurs on the flank face of TC tool after 1000 m cutting compared with the CC tool. The lowest minimum flank wear VB_{max} is obtained by TC-MN tool, which are reduced by ~45% compared with that of CC tool, as shown in Fig. 14a. On the other hand, although the CT-M tool presents a higher VB_{max} value compared with the CC tool, the VB_{max} of CT-N and CT-MN tool
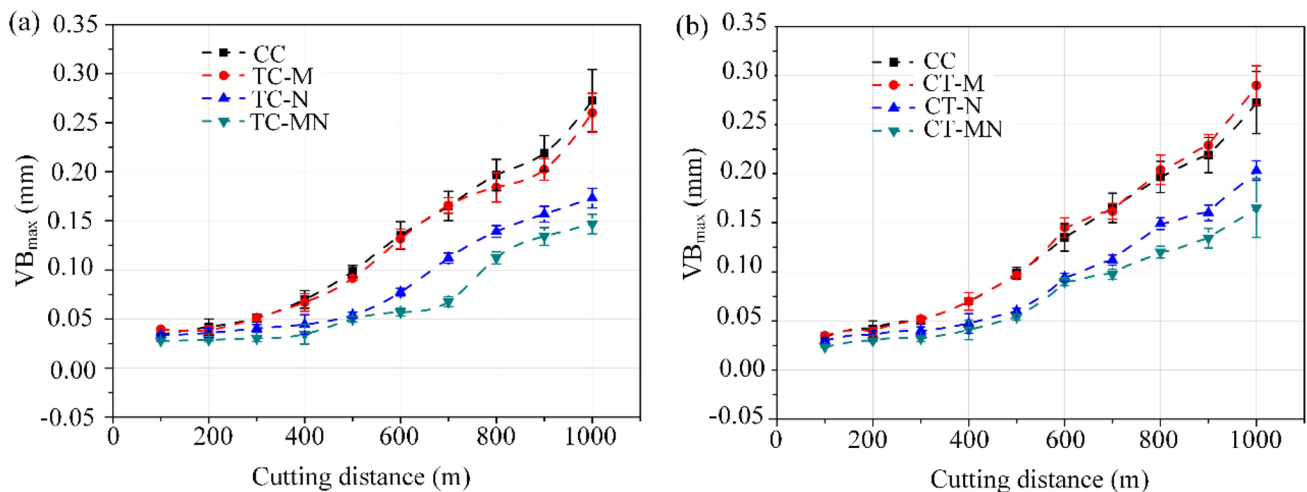

Fig. 14 The maximum flank wear VB_{max} as a function of cutting distance of different tools at speed of 200 m/min

are also reduced (Fig. 14b). These results keep well with that detected by SEM/EDS.

3.3.3 Mechanism for the Effect of Texture Dimension and Sequence

Through the above results it can be found that the anti-adhesive wear properties of TiAlN coated tool in dry cutting of the SLM-produced stainless steel is effectively improved by laser surface texturing. To note, sequence of surface texturing has a great effect on the mechanical properties and cutting performance of coated tools. The developed cutting tools which are textured before TiAlN coating deposition (TC) are more effective in improving the coating adhesion and anti-adhesive wear properties compared to the developed cutting tools which are textured after TiAlN coating deposition (CT), as shown in Figs. 7 and 14. In case of CT samples, a massive oxidation and accumulating of molten TiAlN coatings materials occurs due to the degradative thermal effect, which even can degrade the mechanical properties of the TiAlN coatings surface and consequently decrease the bonding property, as shown in Fig. 7. For TC tools, the wear behavior of TiAlN coatings against SLM-produced stainless steel are obviously promoted by laser

textured substrates. As presented in Figs. 9, 10 and 11, the adhesion of workpieces to the TiAlN coatings surface repeatedly leads to the involved adhesive wear of coated tool here, and the subsequent flaking of the weakly bonded coatings occurs. The phenomenon of coatings detachment from the substrate surface can be relieved by a high adhesive strength between the coatings and substrate. Thus, the high coating adhesion due to the laser surface texturing before coatings is the reason why the TC tools presents better anti-adhesive wear properties than the CC and CT tools. As the residual stress within the substrate surface layer can affect the initiation and propagation of coating cracks and interface delamination, the residual stress measurements at different substrate surface are needed. Owing to the laser processing prior coating, a high compressive stress of substrate surface is achieved regardless of the texturing dimension (Fig. 8), which can support and fit on the subsequent deposited TiAlN coatings. In addition, the textured substrate can provide a higher effective contact area for the subsequent coating deposition than the untextured substrate. Therefore, a larger adhesive strength is caused by the improved mechanical bonding interface between coatings and substrate, as shown in Fig. 15. Besides the residual stress and topography, surface reactivity of the substrate has also an effect on the

Fig. 15 The schematic illustration on the mechanisms for the effects of laser texturing before coatings
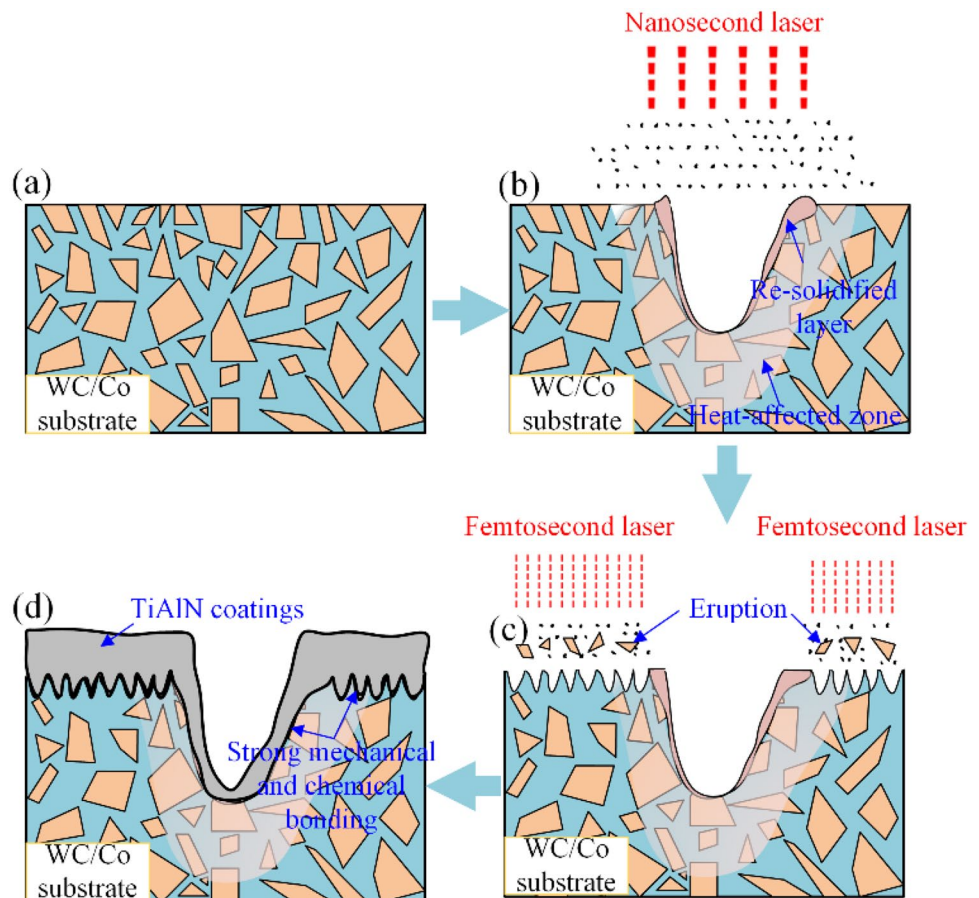
coating adhesion. For PVD TiAlN coatings, the improved surface wettability of substrate can achieve the increasing of coating adhesion. Wettability angles observed from the perpendicularly to the groove direction are 52.54°, 41.50°, and 27.84° for the micro-, nano- and micro/nano-textured substrates, respectively. And, the equilibrium contact angle of untextured substrate is 76.5°. It can be seen that the laser treatment increases the hydrophilicity, and the best wettability is obtained by the micro/nano-textured substrate surface. Well known, chemical reactions at the interface leading to covalent chemical bonds between the coatings and substrate are required for the adequate coating adhesion, which means that the highly reactive functional substrate surface is necessary for the subsequent coating deposition. During laser irradiation, the melting and evaporating of Co binder phase on substrate surface can inhibit the formation of non-TiAlN phase at the interface and promote the formation of strong chemical bonding interface between the coatings and substrate, as shown in Fig. 15. Therefore, the laser surface texturing is also effective for enhancing the surface free energy of WC/Co substrate, which results in an increased coating adhesion.

4 Conclusions

In this work, different scale textures are successfully fabricated on WC/Co cemented carbide cutting tools before and after PVD TiAlN coatings deposition, and the effect of dimension and sequence of surface textures on the anti-adhesive wear properties of PVD TiAlN coated tools during dry cutting SLM-produced stainless steel is studied. The coatings detachment of the textured TiAlN coated tools after cutting tests are smaller than that of the untextured one, and the flank wear VB_{max} of the developed tool which is micro/nano-textured before TiAlN coatings is reduced by ~45% compared with that of the untextured one. Thus, the anti-adhesive wear performance of the textured TiAlN coated tools is obviously improved. The wear resistance of textured TiAlN coated tools presents a strong correlation with texture dimension, and the developed tool with micro/nano-textures shows the best anti-adhesive properties compared to the tools only with micro- or nano-textures.

The texture sequence has also an obvious effect on cutting performance of TiAlN coated tools. The developed cutting tools which are textured before TiAlN coatings deposition are more effective in improving the coating adhesion and anti-adhesive wear properties compared to the developed ones which are textured after TiAlN coatings deposition, regardless of the textures dimension. This reveals that the laser surface texturing performed on the substrate surface could act as a more effective barrier against flaking of the TiAlN film, provide a higher active surface for the subsequent TiAlN coatings and present a higher compressive residual stress, consequently improving the cutting performance of PVD TiAlN coated tools in dry machining of SLM-produced stainless steel.

Compliance with Ethical Standards

Conflict of interest On behalf of all authors, the corresponding author states that there is no conflict of interest.

References

1. Yap, C. Y., Chua, C. K., Dong, Z. L., Liu, Z. H., Zhang, D. Q., Loh, L. E., et al. (2015). Review of selective laser melting: Materials and applications. *Applied Physics Reviews, 2*, 041101.
2. Abdoos, M., Yamamoto, K., Bose, B., Fox-Rabinovich, G., & Veldhuis, S. (2019). Effect of coating thickness on the tool wear performance of low stress TiAlN PVD coating during turning of compacted graphite iron (CGI). *Wear, 422–423*, 128–136.
3. Long, Y., Zeng, J. J., & Wu, S. H. (2014). Cutting performance and wear mechanism of Ti–Al–N/Al–Cr–O coated silicon nitride ceramic cutting inserts. *Ceramics International, 40*, 9615–9620.
4. Zhang, Q., Xu, Y. X., Zhang, T. F., Wu, Z. T., & Wang, Q. M. (2018). Tribological properties, oxidation resistance and turning performance of AlTiN/AlCrSiN multilayer coatings by arc ion plating. *Surface and Coatings Technology, 356*, 1–10.
5. Pfeiler, M., Kutschej, K., Penoy, M., Michotte, C., Mitterer, C., & Kathrein, M. (2007). The influence of bias voltage on structure and mechanical/tribological properties of arc evaporated Ti–Al–V–N coatings. *Surface and Coatings Technology, 202*, 1050–1054.
6. Pfeiler, M., Fontalvo, G. A., Wagner, J., Kutschej, K., Penoy, M., Michotte, C., et al. (2008). Arc evaporation of Ti-Al-Ta-N coatings: The effect of bias voltage and Ta on high-temperature tribological properties. *Tribology Letters, 30*, 91–97.
7. Pfeiler, M., Mayrhofer, P. H., Chladil, K., Penoy, M., Michotte, C., Kathrein, M., et al. (2015). Effect of wavelength modulation of arc evaporated Ti–Al–N/Ti–Al–V–N multilayer coatings on microstructure and mechanical/tribological properties. *Thin Solid Films, 581*, 20–24.
8. Castanho, J. M., & Vieira, M. T. (2003). Effect of ductile layers in mechanical behaviour of TiAlN thin coatings. *Journal of Materials Processing Technology, 143–144*, 352–357.
9. Kutschej, K., Mayrhofer, P. H., Kathrein, M., Polcik, P., & Mitterer, C. (2005). Influence of oxide phase formation on the tribological behavior of Ti-Al-V-N coatings. *Surface and Coatings Technology, 200*, 1731–1737.
10. Kromer, R., Costil, S., Cormier, J., Courapied, D., Berthe, L., Peyre, P., et al. (2015). Laser surface patterning to enhance adhesion of plasma sprayed coatings. *Surface and Coatings Technology, 278*, 171–182.
11. Li, S. P., Deng, J. X., Yan, G. Y., Zhang, K. D., & Zhang, G. D. (2014). Microstructure, mechanical properties and tribological performance of TiSiN–WS$_2$ hard-lubricant coatings. *Applied Surface Science, 309*, 209–217.

12. Buchwalder, A., & Zenker, R. (2019). Pre- and post-surface treatments using electron beam technology for load-related application of thermochemical and PVD hard coatings on soft substrate materials. *Surface and Coatings Technology, 375*, 920–932.

13. Tillmann, W., Hagen, L., Stangier, D., Krabiell, M., & Elbers, M. (2019). Influence of etching-pretreatment on nano-grained WC-Co surfaces and properties of PVD/HVOF duplex coatings. *Surface and Coatings Technology, 374*, 32–43.

14. Lian, Y. S., Chen, H. F., Mu, C. L., Deng, J. X., & Lei, S. (2018). Experimental investigation and mechanism analysis of tungsten disulfide soft coated micro-nano textured self-lubricating dry cutting tools. *International Journal of Precision Engineering and Manufacturing-Green Technology, 5*, 219–230.

15. Lamraoui, A., Costil, S., Langlade, C., & Coddet, C. (2010). Laser surface texturing (LST) treatment before thermal spraying: A new process to improve the substrate-coating adherence. *Surface and Coatings Technology, 205*, 164–167.

16. Zheng, X. H., Tan, J., & Zhang, Q. (2017). Effect of laser surface texturing depth on the adhesion of electroless plated nickel coating on alumina. *Surface and Coatings Technology, 311*, 151–156.

17. Yuan, S., Lin, N. M., Zou, J. J., Liu, Z. Q., Wang, Z. X., Tian, L. H., et al. (2019). Effect of laser surface texturing (LST) on tribological behavior of double glow plasma surface zirconizing coating on Ti6Al4V alloy. *Surface and Coatings Technology, 368*, 97–109.

18. Neves, D., Diniz, A. E., & Lima, M. S. F. (2013). Microstructural analyses and wear behavior of the cemented carbide tools after laser surface treatment and PVD coating. *Applied Surface Science, 282*, 680–688.

19. Viana, R., Lima, M. S. F., Sales, W. F., Jr., da Silva Junior, W. M., & Machado, Á. R. (2015). Laser texturing of substrate of coated tools-performance during machining and in adhesion tests. *Surface and Coatings Technology, 276*, 485–501.

20. Enomoto, T., & Sugihara, T. (2010). Improving anti-adhesive properties of cutting tool surfaces by nano-/micro-textures. *CIRP Annals-Manufacturing Technology, 59*, 597–600.

21. Sugihara, T., & Enomoto, T. (2012). Improving anti-adhesion in aluminum alloy cutting by micro stripe texture. *Precision Engineering, 36*, 229–237.

22. Zhang, K. D., Guo, X. H., Sun, L. N., Meng, X. F., & Xing, Y. Q. (2019). Fabrication of coated tool with femtosecond laser pretreatment and its cutting performance in dry machining SLM-produced stainless steel. *Journal of Manufacturing Processes, 42*, 28–40.

23. Zhong, Y., Liu, L. F., Wikman, S., Cui, D. Q., & Shen, Z. J. (2016). Intragranular cellular segregation network structure strengthening 316L stainless steel prepared by selective laser melting. *Journal of Nuclear Materials, 470*, 170–178.

24. Zhang, K. D., Deng, J. X., Xing, Y. Q., Li, S. P., & Gao, H. H. (2015). Effect of microscale texture on cutting performance of WC/Co-based TiAlN coated tools under different lubrication conditions. *Applied Surface Science, 326*, 107–118.

25. Rossnagel, S. M., & Cuomo, J. J. (1989). Film modification by low energy ion bombardment during deposition. *Thin Solid Films, 171*, 143–156.

26. Semaltianos, N. G., Perrie, W., French, P., Sharp, M., Dearden, G., & Watkins, K. G. (2008). Femtosecond laser surface texturing of a nickel-based superalloy. *Applied Surface Science, 255*, 2796–2802.

27. Zhang, K. D., Deng, J. X., Guo, X. H., Sun, L. N., & Lei, S. (2018). Study on the adhesion and tribological behavior of PVD TiAlN coatings with a multi-scale textured substrate surface.

International Journal of Refractory Metals Hard Materials, 72, 292–305.

28. Xu, C. H., Xu, F., Shi, L. L., Gao, J. Y., & Zuo, D. W. (2019). Enhancement of substrate-coating adherence of boron-doped diamond electrodes by nanosecond laser surface texturing pretreatment. *Surface and Coatings Technology, 360*, 196–204.

29. Arroyo, J. M., Diniz, A. E., & Lima, M. S. F. (2010). Wear performance of laser precoating treated cemented carbide milling tools. *Wear, 268*, 1329–1336.

Kedong Zhang Ph. D., Lecturer in the School of Mechanical and Electrical Engineering, Soochow University, Jiangsu, China. His current research interests include cutting tools, green machining and surface engineering for lower friction and wear.

Xuhong Guo is a full professor of the School of Mechanical and Electrical Engineering, Soochow University, Jiangsu, China. His research interests include laser surface textured cutting tools, precision, ultra-precision and high-speed cutting technology, computer simulation of processing technology and forming process of difficult-to-machine materials. He is in charge of the high-speed precision processing technology and equipment research institute at Soochow University.

Chengdong Wang Ph.D., associate professor in the School of Mechanical and Electrical Engineering, Soochow University, Jiangsu, China. His current research interests focus on CFRP, CNC simulation optimization, precision, ultra-precision and high-speed cutting technology.

Xiangfeng Meng was born in Heilongjiang Province, China in 1994. He has been studying for M.S. degree in the School of Mechanical and Electrical Engineering of Soochow University from 2017 to present. His research interests include high-speed precision cutting processing technology, laser processing and coating technology.

Youqiang Xing Ph.D., associate professor in the School of Mechanical engineering, Southeast University, Nanjing, China. His current research interests focus on the cutting tools, green machining and surface engineering for lower friction and wear.

Lining Sun is a Professor in the School of Mechanical and Electrical Engineering, Soochow University, Jiangsu, China. He received the B.S. degree in mechanical engineering, and the M.S. and the Ph.D. degrees in mechatronics engineering from the Harbin Institute of Technology, Harbin, China, in 1985, 1988, and 1993, respectively. His research interests include robot control, micro- and nanorobotics, micromanipulation, nanopositioning actuators, and design and control of high-speed nanopositioning systems.